Extreme ionospheric conditions over Europe observed during the last solar cycle

C. Mayer, N. Jakowski, C. Borries, T. Pannowitsch and B. Belabbas

Christoph.Mayer@dlr.de

German Aerospace Center
Institute of Communications and Navigation

ABSTRACT

The extreme variability of the ionosphere poses a threat to GNSS applications, since the signals of Global Navigation Satellite Systems (GNSS) are influenced by the ionospheric plasma. In this paper we perform a review of ionospheric conditions over Europe using data from the past nine years covering almost the entire solar cycle. We are focusing on parameters important for GNSS applications, such as ionospheric spatial and temporal gradients.

In order to obtain ionospheric gradient information we use both, the total electron content (TEC) rate of change and the differences of calibrated vertical TEC data at the same time. The deduced gradient information is used in order to generate probability density functions. We analyse singular extreme events and investigate correlations between the occurrence of large gradients and geo-physical parameters. Using the November 20, 2003 storm we discuss the potential of TEC gradients for contributing to a meaningful ionospheric perturbation index.

Ionosphere signal delay is one of the major contributors to pseudo range residual error for both absolute positioning and for relative positioning, *e.g.*, in the context of ground-based augmentation systems (GBAS). Our large data set is used in order to generate a generalized model of an instantaneous covariance matrix. The results are compared with a standard covariance matrix and conclusions on its applicability to positioning algorithms will be drawn.

INTRODUCTION

A large dataset of calibrated slant total electron content (TEC) measurements and TEC maps over Europe covering the entire last solar cycle has been generated and archived in DLR Neustrelitz [1], [2]. Using this data, we are able to determine and to quantify statistically both the "normal" ionospheric state and extreme ionospheric events over the European region during the last solar cycle.

Using our TEC maps, we are able to distinguish spatial gradients and temporal variations of TEC at selected grid points of the maps. The TEC rate of change is analysed in a similar way as the spatial ionospheric gradients, *i.e.* the TEC rate of change dependence on geophysical parameters is investigated and the largest observed temporal changes are estimated.

Most ionospheric perturbations are closely related to changes of geomagnetic activity usually described by geomagnetic indices, such as the D_{st} or K_p index. However, as our studies show, there remain a number of ionospheric disturbances which are obviously not related to variations of geomagnetic indices. Thus, to describe the perturbation degree of the ionosphere in a reliable manner, we suggest describing the ionospheric perturbation degree by a specific ionospheric perturbation index.

Since most of current global ionospheric information is obtained thanks to the innovative GNSS technology, it is suggested to use GNSS derived parameters such as TEC for defining such an index. In addition to the high effectiveness of ionospheric monitoring by GNSS measurements, this technique is also sufficiently robust in the presence of ionospheric perturbations. Furthermore, the derived quantities such as TEC are directly usable for mitigating ionospheric range errors in space based positioning and navigation.

It is generally admitted that the ionosphere delay is the dominant effect for absolute positioning receivers [3]. Dual frequency receivers have the possibility to eliminate the ionosphere error; the price for that is an increase of the receiver noise and multipath error [4].

DATA BASIS AND METHODOLOGY

Our data basis consists of calibrated total electron content data, obtained during 2000—2008 from dual-frequency GPS data of about 10-20 GPS receivers distributed over all of Europe. While the input data, which is taken from measurements of IGS stations, has a time resolution of 30 seconds, the processed data is stored with a time resolution of 10 minutes. Details of the pre-processing and calibration procedure can be found in [1].

Physically, the total electron content is given to first order by the integral of the electron density along the ray path from the GPS satellite to the ground station:

$$TEC = \int n_e ds \tag{1}$$

TEC total electron content [m^{-2}]

In the data processing, a single-shell approximation of the ionosphere with height 400 km is used. Thus, for each TEC measurement so-called ionospheric pierce points (IPP) are provided in the form of latitude and longitude of the intersection of the data link with the hypothetical single shell ionosphere.

The TEC values in (1) can be obtained, *e.g.*, from GPS dual-frequency phase observations according to

$$TEC_{slant} \propto L_1 - L_2 + b \tag{2}$$

TEC_{slant} ionospheric range error at L1 band [m]
$L_{1,2}$ phase measurements at GPS band 1,2 [m]
b offset [m]

where we refer the reader to [1] for details of the data processing, except that we would like to point out that since we use phase observables cycle slips have to be corrected, *cf.*, *e.g.*, [5]. Any undetected or unfixed cycle slips or outliers can cause jumps in (2), producing fake large gradients. Note also that it is well-known that especially the L_2-phase observable is more prone to cycle slips than the L_1 observable, especially under disturbed ionospheric conditions.

There are two ways in which one can derive gradient information from (1):

- by forming differences of TEC measured at the same time epoch
- by differencing between adjacent time epochs

In this paper we use both methods. While the first method has the advantage of clearly separating temporal and spatial variations, it is dependent on the precise calibration of TEC and typically provides the bulk of gradients for distances of the order of the distances between the used ground stations. The latter method can provide gradients for very short distances and is independent of the TEC calibration, since only relative variations are considered. However, temporal and spatial variations cannot be separated.

Time differences of TEC are called rate of TEC which is defined by

$$ROT = \frac{\Delta TEC_{slant}}{\Delta t} \tag{3}$$

ROT rate of TEC [m/s]
Δt time difference [s]

where slant TEC differences are taken between subsequent epochs (10 minutes distance) of a link between the same ground station and the same satellite:

$$\Delta TEC_{slant} = TEC_{slant,1} - sTEC_{slant,2} \tag{4}$$

$TEC_{slant,1,2}$ slant TEC values at epochs 1 and 2 [mm]

For the investigations in this paper we use slant TEC gradients derived from ROT in the following way:

$$grad_{ROT} = \frac{\Delta TEC_{slant}}{\Delta s} \tag{5}$$

ΔTEC_{slant} slant TEC difference between two adjacent epochs [mm]
Δs distance of ionospheric pierce points [km]
$grad_{ROT}$ ROT-derived slant gradient [mm/km]=[ppm]

We localize these gradients at the mid-point of the great-circle line between the measurements. Here, Δs denotes the great-circle distance in the ionosphere at 400 km height. For the used time step of 10 minutes, Δs ranges between 31 km and 150 km, with a median value of about 55 km. Since the measurements by which ROT is calculated are taken at different times and different locations, we obtain a mixture between purely temporal and purely spatial gradients which at this point cannot be separated. However, we use the gradients determined by (5) as a tracer in order to detect the large spatial gradients which may pose a threat for GBAS systems. The full analysis of these gradients, which is beyond the scope of this paper, has to include a determination of the velocity of a given ionospheric front in order to properly separate spatial and temporal changes.

Note that the fact that we use data with 10 minutes time resolution does affect the magnitude of the observed gradients. Compared to gradients determined with 30 seconds or higher time resolution, our gradients are lower, since the large time distance smoothes out the steepest gradients. Nevertheless, significant gradients can be observed with 10 minutes time resolution, as we will show below.

In Fig. 1, all ionospheric pierce points representing the location of our measurements during January 2000 and January 2006 are shown. It can be seen that Central Europe is well covered. Data from Northern Europe is provided by stations in Tromsø, Norway, Svalbard and Iceland. There is one station situated on the Canary Islands which provides data from low latitudes below 30° N.

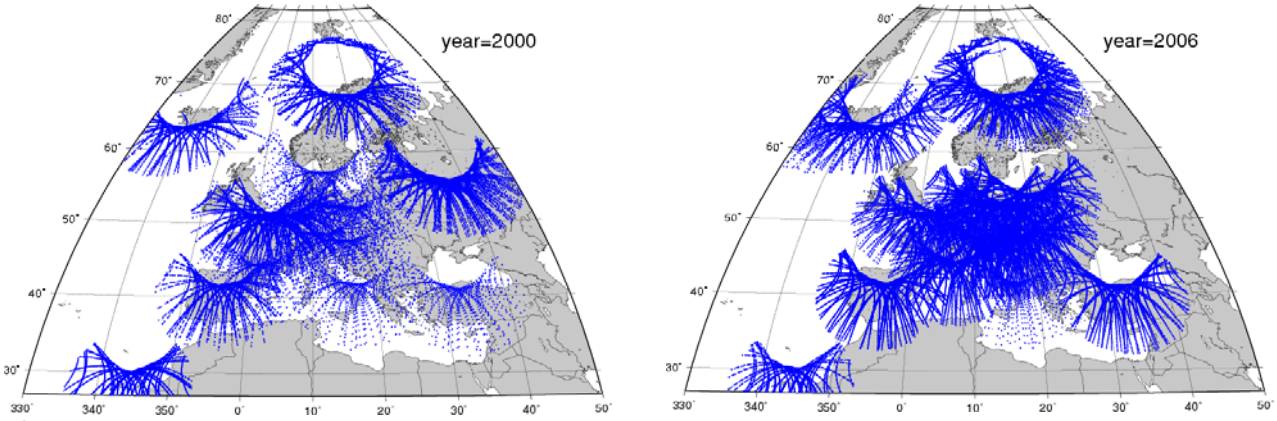

Fig. 1
Ionospheric pierce point locations during January 2000 (left plot) and January 2006 (right plot).

EXTREME EVENTS OBSERVED

Gradient pdf

In order to obtain an overview over the observed gradients, we start by computing the probability density function (pdf) of all gradients computed according to (5) in the period from 2000—2008 using more than 10^7 data points. Note that the pdf shown below is an *overbound* to the true pdf of ROT-derived gradients, since deficiencies in the data processing can easily generate fake large gradients. Up to ca. ±25 ppm $\log_{10}$(pdf) drops almost linearly; above ±25 ppm the descent is less steep and there are tails below the 10^{-7}-level coming from the most extreme events observed. Note again that these gradients are computed from time differences of slant TEC with 10 minutes separation; gradients seen at smaller time differences will be certainly higher.

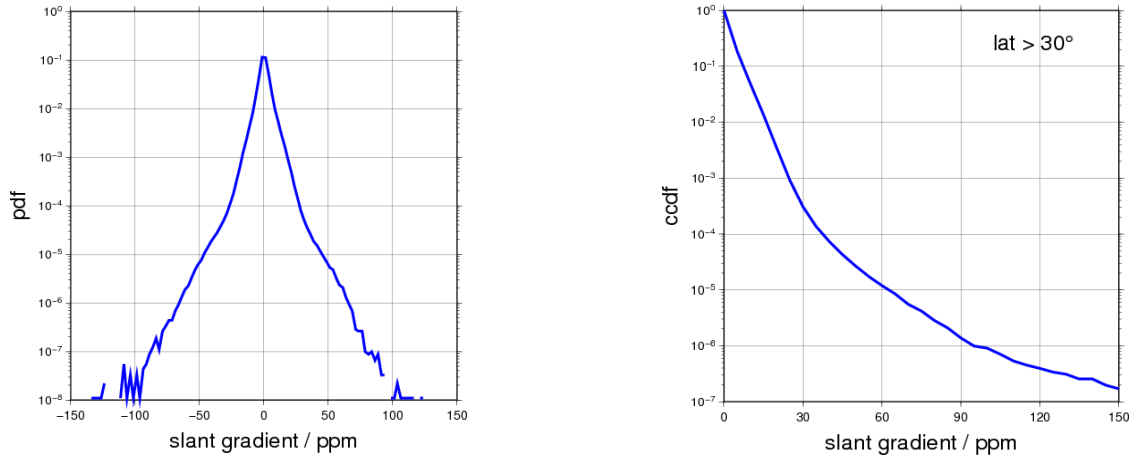

Fig. 2
The left plot displays the pdf of ROT-derived slant gradients computed according to (5) for the entire data set spanning nine years 2000—2008. On the right hand side the complementary cumulative distribution function (ccdf) is shown for all ROT-derived slant gradients observed above 30° N.

Latitude dependence

The distribution of observed ROT-derived gradients with respect to date and latitude is shown in Fig. 2, where we have plotted all gradients exceeding a certain threshold.

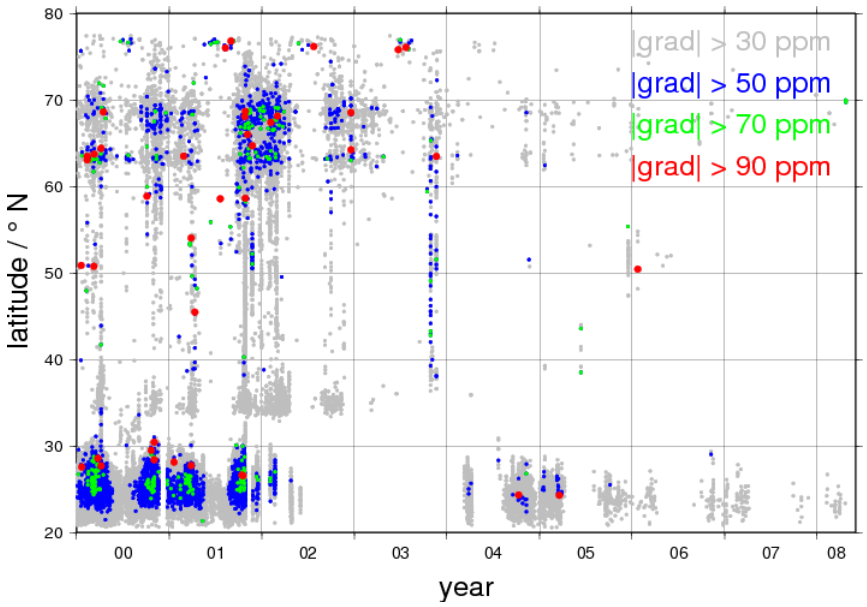

Fig. 3
Latitudinal distribution of the location of ROT-derived slant gradients exceeding 30, 50, 70, and 90 ppm during 2000 – 2008

First, we note that large gradients are more numerous during the solar maximum in 2000—2002. While large gradients occur quite regularly below 30°N, for latitudes bigger than 30° N large gradients show a more patchy structure and occur mostly in and above the aurora zone at latitudes north of 60° N.

Below 30° N medium size large gradients (i.e. less than 70 ppm) show a pronounced regular seasonal pattern, with peaks during the spring and autumn equinoxes. Note that between mid 2002 and beginning of 2004 no data was collected from the relevant station. The consistently high gradients observed below 30° N are most likely due to the crest of the Equatorial Anomaly, since there is a pronounced azimuth dependence of large gradients observed below 30° N, *cf.* Fig. 4. These large gradients are observed in southern directions mostly.

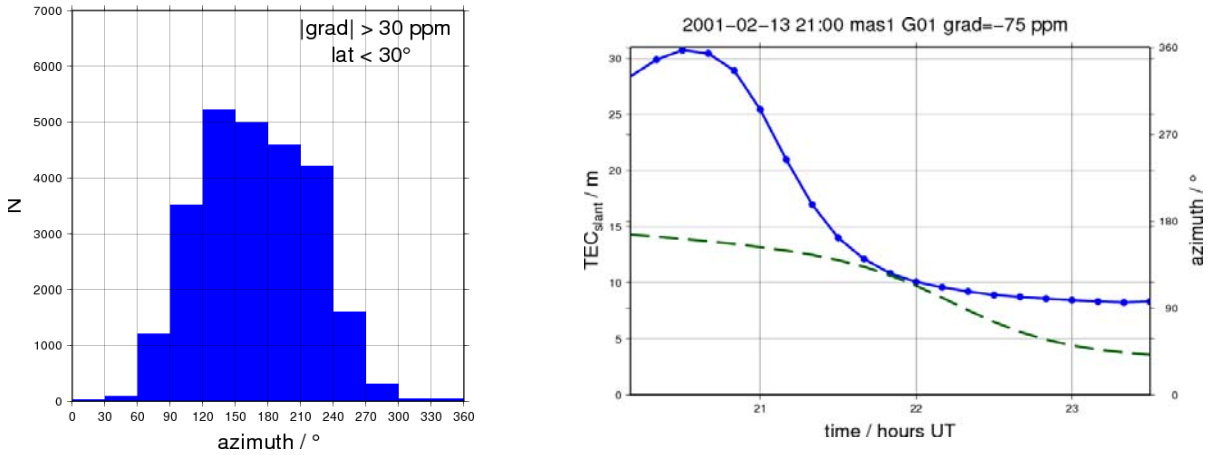

Fig. 4

Histogram of ROT- derived slant gradients bigger than 30 ppm observed at latitudes less than 30° N (left panel). These gradients are seen predominantly in southerly directions, pointing to the equatorial crest phenomenon as an explanation. On the right hand side, sample slant TEC values are shown in blue, measured by an IGS stations on the Canary Islands; the dashed line shows the azimuth of the measurements. Clearly when looking to the south (180° azimuth) quite high slant TEC values are seen. The gradient of -75 ppm is due to the steep slope of the slant TEC curve.

The ionospheric storm on November20, 2003

As an example of a day characterized by large observed gradients we select the ionospheric storm on November 20, 2003. On this day, large ionospheric gradients were observed from two stations in Iceland. First we present a preliminary analysis of the moving ionospheric front which caused these large gradients, then we analyse the same event for discussing the potential of spatial TEC gradients for defining an ionospheric perturbation index.

Single Gradient Analysis

The analysis with our data with 10 minute time resolution has indicated a gradient of ca. -100 ppm. A more careful analysis using 30 second data is presented in Fig. 5 which shows that the actual gradients are as high as -200 ppm. A preliminary analysis of this large gradient using data of three GPS receivers (two on Iceland, one on Faroe Island) shows that it can be modelled as a moving ionospheric front, according to the GBAS CAT-I ionosphere threat model [7], [8]. Using a least-squares-based estimation method, the velocity of this front has been found to be 2 m/s in East-West direction and 117 m/s in North-South direction. Thus the front propagated from North to south at a speed of 117 m/s.

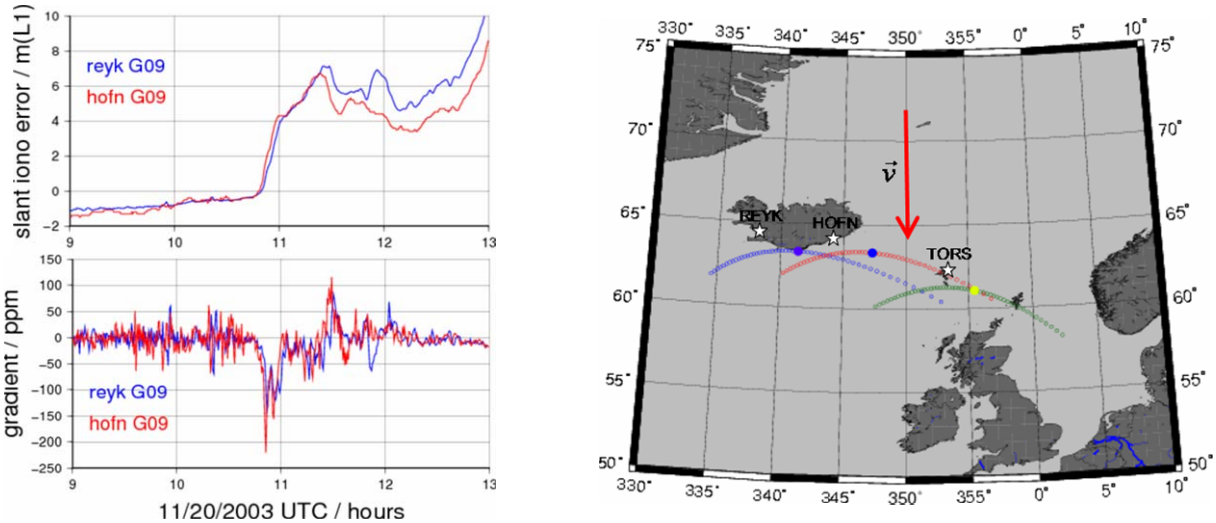

Fig. 5

Left: The top plot shows the relative slant ionospheric error on L1 obtained from GPS phase-difference measurements with 30 second resolution for two stations on Iceland. The bottom plot displays the apparent slant gradients in ppm.
Right: the IPP traces seen from the three used receivers, indicated as white stars, are shown as empty circles, the location of the observed maximal gradients are shown as full circles and the estimated velocity as an arrow.

Ionospheric Perturbation Index

As shown earlier in [9], spatial gradients of TEC may provide significant information on the perturbation degree of the ionosphere during ionospheric storms. Furthermore, the knowledge of spatial TEC gradients is important in precise GNSS positioning and safety-critical GNSS applications in aviation. Thus, it was suggested to consider spatial TEC gradients as an essential contributor for the estimation of an ionospheric perturbation index which can effectively be used in GNSS applications.

To evaluate former conclusions we have analysed the spatial gradients of vertical TEC directly between sub-ionospheric or piercing points of GPS satellite-ground station links during each individual epoch at severe perturbation periods. Whereas the gradient computation discussed in [9] uses a regular grid impacted by interpolation and smoothing algorithms, the gradient computation between piercing points is more original. Nevertheless, some rest errors due to the simplicity of the applied single layer mapping function and the calibration procedure cannot be excluded.

Having in mind that spatial gradients are a good candidate for defining an ionospheric perturbation index we have estimated regional ionospheric disturbance indices (RIDX) by averaging all values whose gradient location (central point between two piercing points) lie within a certain map area. Thus, for Europe we have defined nine regions consisting of three longitude sectors from 15°W – 30°E with 15° width and three latitude zones from 35°N – 65°N with 10° width, respectively. The averaged spatial gradients of vertical TEC given in mm/km for the L1 GPS frequency are considered as exclusive RIDX contributors for the different regions.

The temporal development of these parameters for the central European longitude sector 0°E – 15°E is shown in Fig. 6 at the different latitude zones for the storm on November 20, 2003. It is interesting to note that the TEC_v gradients are growing up to 4 mm/km during the storm characterized by the geomagnetic ap and D_{st} indices [10] clearly indicating the space weather relationship of the gradients. A prominent feature is also a significant time delay of the perturbation pattern from higher toward lower latitudinal zones. This finding is obviously related to the preferred equatorward propagation of ionospheric disturbances which is underlined by the observed asymmetry of the spatial gradients pronouncing the North- South direction by a factor of about 1.5 as shown in Fig. 6. Both these observation need further investigation indicating a great potential for quantitatively describing the perturbation degree of a certain area by a regional RIDX.

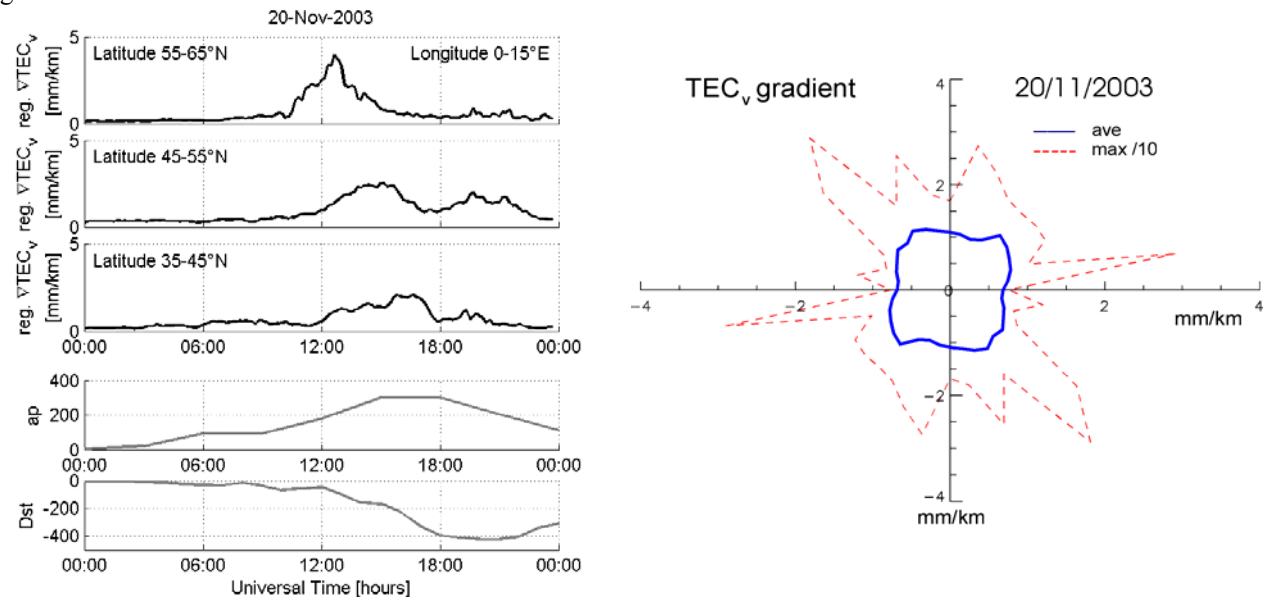

Fig. 6
Left plot: Spatial gradients of vertical TEC averaged in the 0°E—15°E longitude sector at three different latitude zones (upper panels) on 20 November 2003. Comparison is made with geomagnetic indices such as ap and D_{st} (lower panels).

Right plot: Polar plot of the azimuthal distribution of horizontal vertical TEC (TEC_V) gradients (resolution 10°) on November 20, 2003: full line - average values of all observations during the entire day, dashed line – extracted maximum values reduced by a factor of 0.1.

In the next section we turn to investigate the relationship between geo-physical parameters and large ionospheric gradients on a statistical basis by using the data of the last nine years.

GEO-PHYSICAL RELATIONSHIPS

In order to study the connection between geomagnetic indices and the occurrence of large ionospheric gradients we use two indices: the A_p index which is sensitive to geomagnetic disturbances, and the solar F10.7 radio flux which is a measure of solar activity. As can be already seen from Fig. 3, the large gradients below 30°N are mostly sensitive to the solar activity, while the gradients above 30° N are more frequent at high solar activity, but also much more irregular, linked to geomagnetic disturbances. These observations can be found in the scatter plots of Fig. 7 and Fig. 8, too.

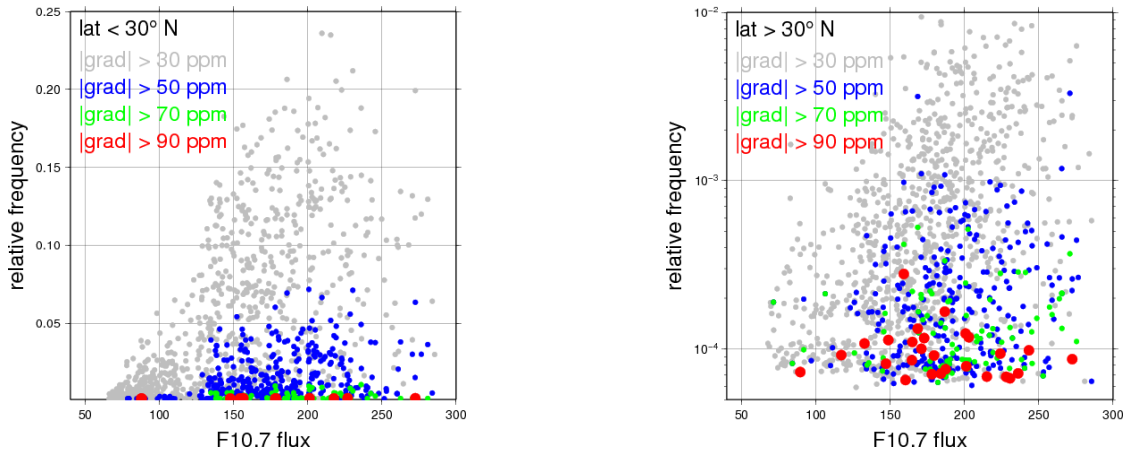

Fig. 7
Relationship between the relative frequency of large gradients and the solar F10.7 radio flux for gradients below (right plot) and above (left plot) 30° N.

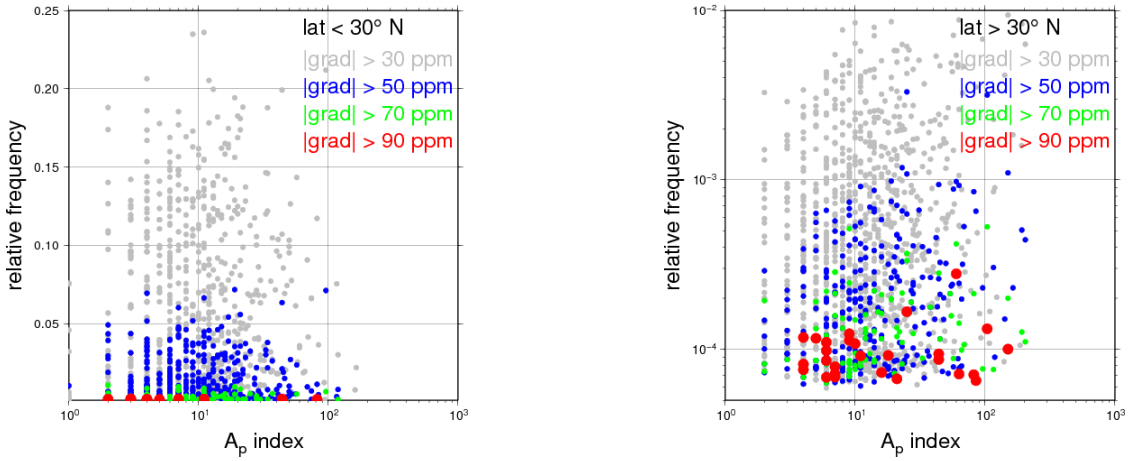

Fig. 8
Relationship between the relative frequency of large gradients and the geomagnetic A_p index for gradients below (right plot) and above (left plot) 30°N.

We see that large gradients below and above 30° N show a different behaviour with respect to the A_p index and the F10.7 radio flux:

- Below 30° N large gradients do not correlate with Ap, but show a positive correlation with F10.7. This is consistent with the fact that these gradients are due to the Equatorial Anomaly the strength of which mostly depends on solar activity.

- Above 30° N, we find a weak positive correlation with solar activity, especially for medium size gradients. As expected, there is a positive correlation with geomagnetic activity, which is most clear for the biggest observed gradients.

GENERALIZED COVARIANCE MATRIX

Local differential GNSS (using single frequency code measurements) provides the most accurate non carrier phase based solution. The ionosphere delay is reduced to a large amount and only the de-correlated part of it remains. This is represented by the spatial ionosphere gradient as represented in the left graphic below.

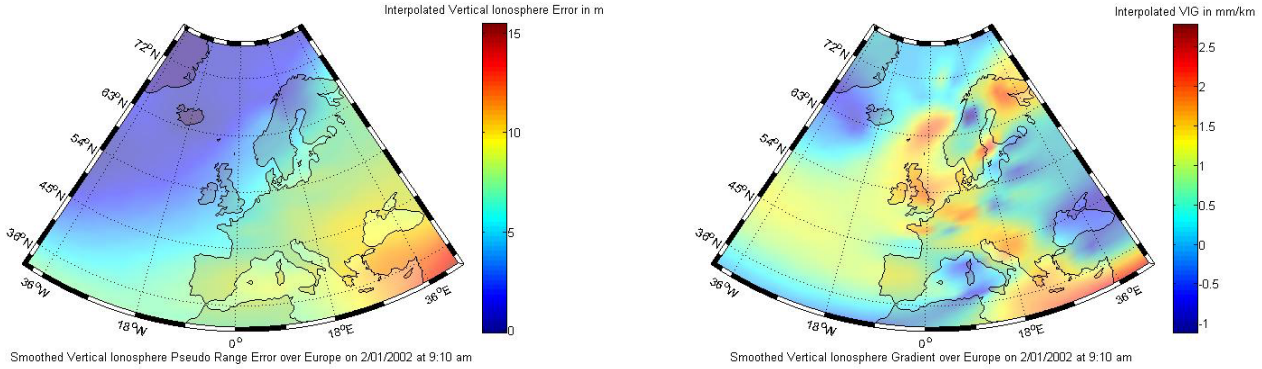

Fig. 9
Vertical ionosphere error map (left) and vertical ionosphere gradient map (right) over Europe.

Fig. 9 represents a snapshot of the vertical ionosphere map and the vertical ionosphere gradient map obtained by using vertical TEC values obtained from different IGS stations distributed all over Europe. The data were interpolated and regularly redistributed in a grid. The grid is defined by a 30•50 array of points. These values correspond to a time instant on January 2, 2002. The error calculated in the left graphic corresponds to the errors impacting the L1 frequency of a GNSS signal. The vertical ionosphere gradient responsible of the residual ionosphere error for GBAS corresponds to a "normal" behaviour of the ionosphere gradient ranging from -1.2 to +2.7 mm/km.

Thanks to 4 months of vertical TEC and vertical TEC gradient measurements all over Europe, it was possible to determine the cross covariance between different points of the grid. Fig. 10 represents the spatially covariance space generated by the point in the middle of the grid. The covariance space concept is well defined in [11].

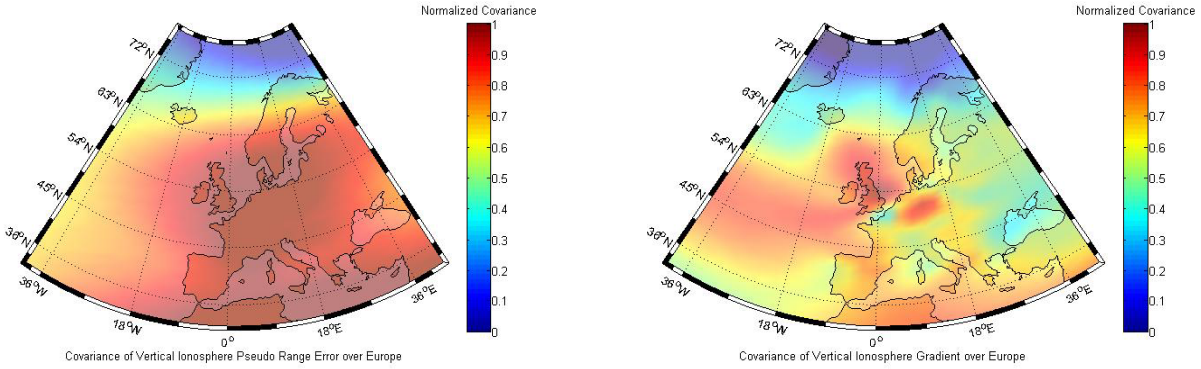

Fig. 10
Shown is the generalized covariance space of the vertical ionosphere error (left) and gradient (right) over Europe.

For convenience, the covariance terms have been normalized by the variance at reference point (middle of the map). The red area represents strongly correlated values. The results are interesting: for single frequency absolute positioning the ionosphere error is spatially strongly correlated which has very high consequences in the calculation of the user position. For the differential case (see the left graphic), the gradient is still correlated but with a lower amount. It can be concluded for this chapter that the differential process not only reduces the ionosphere residual error but reduces also the spatially correlated part of the ionosphere. As a consequence of this result for differential applications, there is an improvement in user level error delectability.

CONCLUSIONS

In this paper we have analysed the occurrence ionospheric gradients during the last solar cycle using data from the years 2000—2008. For this analysis we used gradients determined from slant TEC rate of change and gradients determined from vertical TEC at same times.

We find that gradients below 30° N are due to the Equatorial Anomaly. These gradients occur during the spring and autumn equinoxes and are correlated with the solar F10.7 radio flux. In contrast, gradients above 30° N, show only a weak correlation with the solar F10.7 radio flux. However, large gradients correlate with the geomagnetic A_p index.

Using gradients determined from TEC rate of change, we were able to determine gradient pdfs and ccdfs using more than 10^7 measurements. Thus we come somewhat close to the order of magnitude of probabilities used in aviation requirements [12]. In addition, we have analysed the storm of Nov 20 2003 with respect to a singular large gradient observed over Iceland, and as an example of how to make up an ionospheric perturbation index.

Further work will investigate generalized covariance matrices for the ionospheric contribution. An application for both absolute and differential modes is the possibility to generalize the weighting matrix by considering it not anymore as diagonal but by taking into account the covariance terms. An impact on integrity of a generalized covariance matrix has been already presented in [11] for a global error.

ACKNOWLEDGEMENTS

CM, NJ, CB, and TP gratefully acknowledge support of the German state government of Mecklenburg-Vorpommern under the grant number AU-07008 (SWACI). We also acknowledge the International GNSS Service (IGS) for making available the use of GPS data over many years, the NOAA/National Geophysical Data Center (NGDC) in Boulder for free provision of A_p and F10.7 indices via their ftp service, and the World Data Center for Geomagnetism in Kyoto for free provision of D_{st} index data.

REFERENCES

[1] Jakowski, N., TEC Monitoring by Using Satellite Positioning Systems, in Modern Ionospheric Science, (Eds. H. Kohl, R. Rüster, K. Schlegel), EGS, Katlenburg-Lindau, ProduServ GmbH Verlagsservice, Berlin, pp 371-390,1996

[2] SWACI: Space Weather Application Center Ionosphere, http://w3swaci.dlr.de

[3] Belabbas, B. Petitprez, F., Hornbostel, A., UERE Analysis for Static Single Frequency Frequency Positioning using Data of IGS Stations, Proceedings of the ION National Technical Meeting, 2005

[4] Sadeque, M. Z., Implementation of UERE Module into NAVSIM and Study of Errors for Single and Dual Frequency GPS-Receivers, Master Thesis, Chalmers University of Technology, 2005

[5] Blewitt, G., 1990. An automatic editing algorithm for GPS data. Geophys. Res. Lett. 17, pp. 199-202.

[6] Jakowski , N., R. Leitinger, and L. Ciraolo, Behaviour of large scale structures of the electron content as a key parameter for range errors in GNSS applications, Annals of Geophysics, Supplement to Volume 47, N. 2/3, 2004, pp. 1031-1047, 2004

[7] Lee, Jiyun, Luo, M. Pullen, S., Park, Y. S., Enge, P., and Brenner, M. Position-Domain Geometry Screening to Maximize LAAS Availability in the Presence of Ionosphere Anomalies Presented September 2006 at the ION Institute of Navigation Global Navigation Satellite Systems Conference, Fort Worth, TX

[8] Shankararaman Ramakrishnan, Jiyun Lee, Sam Pullen, and Per Enge, Targeted Ephemeris Decorrelation Parameter Inflation for Improved LAAS Availability during Severe Ionosphere Anomalies Presented January 2008 at the ION Institute of Navigation National Technical Meeting, San Diego, CA

[9] Jakowski, N., S.M. Stankov, S. Schlüter, D. Klähn, On developing a new ionospheric perturbation index for space weather operations, Adv. Space Res., doi: 10.1016/j.asr.2005.07.043, 2005

[10] NOAA/NGDC ftp://ftp.ngdc.noaa.gov/STP/GEOMAGNETIC_DATA/INDICES/KP_AP, World Data Center for Geomagnetism, Kyoto D_{st} index service, http://swdcwww.kugi.kyoto-u.ac.jp/dstdir/index.html

[11] Belabbas, B., Gass, F., RAIM Algorithms Analysis for a Combined GPS/GALILEO Constellation, Proceedings of the ION GNSS 2005

[12] Minimum Operational Performance Specification For Global Navigation Satellite Ground Based Augmentation System Ground Equipment To Support Category I Operations, ED-114, Eurocae, Paris, September 2003